The P-wave velocity structure of Deception Island, Antarctica, from two-dimensional seismic tomography

T. Ben-Zvi,[1] W. S. D. Wilcock,[2] A. H. Barclay,[3] D. Zandomeneghi,[4] J. M. Ibáñez,[4] J. Almendros,[4] and Tomodec Working Group

[1]Department of Earth and Space Sciences, University of Washington, Box 351310, Seattle, WA 98195-1310. (E-mail: tbenzvi@u.washington.edu)
[2]School of Oceanography, University of Washington, Box 357940, Seattle, WA 98195-7940.
[3]Lamont-Doherty Earth Observatory, Palisades, NY 10964.
[4]Instituto Andaluz de Geofísica, University of Granada, Campus de Cartuja,s/n, Granada, 18071 Spain.

Summary Deception Island is a volcanic island with a flooded caldera that has a complex geological setting in Bransfield Strait, Antarctica. We use P-wave arrivals recorded on land and seafloor seismometers from airgun shots within the caldera and around the island to invert for the P-wave velocity structure along two orthogonal profiles. The results reveal a low-velocity anomaly beneath the caldera with a maximum anomaly of ~-1 km/s extending from the seafloor to ~5 km depth. Refracted arrivals suggest a >1-km-thick layer of sediments and unconsolidated lavas infilling the caldera. Synthetic inversions show that this layer accounts for only a small portion of the velocity anomaly, implying that there is a significant region of low velocities at greater depths. Further synthetic inversions and melt fraction calculations suggest that the caldera is underlain by an extensive region of magma that extends downwards from <2 km beneath the seafloor.

Citation Ben-Zvi, T., W. S. D. Wilcock, A. H. Barclay, D. Zandomeneghi , J. M. Ibáñez, and J. Almendros, The P-Wave velocity structure of Deception Island, Antarctica, from two-dimensional seismic tomography, in Antarctica: A Keystone in a Changing World – Online Proceedings of the 10th ISAES X, edited by A. K. Cooper and C. R. Raymond et al., USGS Open-File Report 2007-1047, Extended Abstract 078, 5 p.

Introduction

Deception Island is an active strato-volcano at the south-west end of Bransfield Strait, a backarc basin that developed between the South Shetland Islands and the Antarctic Peninsula (Figure 1a). The South Shetland island arc formed as the result of the subduction of the Phoenix plate beneath the Antarctic plate. The rate of subduction decreased dramatically at about ~4 Ma (Barker, 1982) and continues today, if at all, only very slowly (Robertson et al., 2002). The Bransfield Strait backarc basin is still undergoing extension (Barker, 1982) and is characterized by a series of asymmetric basins with well-delineated volcanic rifts. Deception Island forms the boundary between the Central and Western Bransfield Basins and its footprint extends from the axis of back arc extension to the northeastern boundary of the basin.

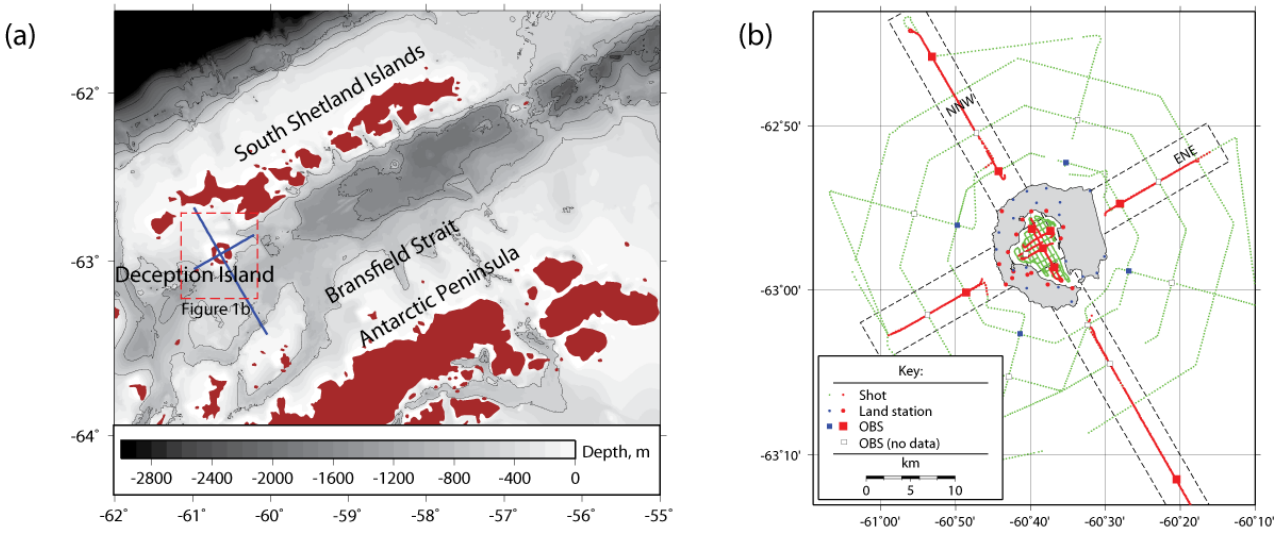

Figure 1. (a) Location of Deception Island and the seismic refraction profiles (blue lines) in Bransfield Strait. The boundaries of extension on either side of the Strait are delineated by the bathymetry. (b) Experiment design showing the location of seismic stations and arrays on land (circles), ocean bottom seismometers (squares), and airgun shots for the first round of shooting (dots). Larger symbols in corridors that are enclosed by dashed lines show the stations and shots used for two-dimensional inversions.

The emerged top of the volcano is a small horseshoe shaped island with a diameter of ~15 km that encircles a flooded caldera measuring 5-9 km across with a narrow opening to the sea. The volcano has erupted several times historically, most recently in a series of small eruptions in 1967-1970 (Smellie, 2001). Its age is poorly constrained but

estimated from magnetic polarities to be <500 Ka (Smellie et al., 2002). It has a mean composition of basaltic-andesite to basalt and enigmatic petrological characteristics that indicate both arc and backarc influences (Smellie et al., 2002).

Deception Island's caldera has traditionally been considered a classic volcanic collapse caldera (Baker et al., 1975), although extensive deposits from the caldera forming eruption have yet to be identified. Motivated in part by the lack of evidence for the formative eruption, Marti et al.(1996) interpreted fault patterns around the caldera in terms of an alternative model in which the caldera formed as a passive response to regional extension in two directions. More recently, Smellie et al. (2002) have cited petrological evidence to support a model in which extension promoted the mixing of two magma types and an explosive instability. They estimate the size of the caldera forming eruption to be ~ 30 km^3.

Bransfield Strait and environs have been the have focus of many regional-scale seismic experiments that have sought to understand the structure of the backarc rift and the tectonics of the region (e.g., Barker et al., 1998; Christeson et al., 2003; Grad et al., 1997; Robertson et al., 2002). However, on Deception Island itself, seismic experiments have been limited to shallow seismic reflection (Rey et al., 2002) and refraction (Grad et al., 1992) imaging of sediment layers in the caldera and to the deployment of small networks and arrays for monitoring earthquakes and emergent signals (e.g., Ibanez et al., 2003). The only constraints on deeper structure have come from potential field (Muñoz-Martín et al., 2005) and geothermal observations (Ortiz et al., 1991) that have been used to infer the presence of shallow magma.

Because the caldera of Deception Island is accessible to research ships, it is an ideal setting for a seismic tomography experiment that combines airgun shooting in the caldera and around the island with a dense network of land stations and deployments of ocean bottom seismometers. In this paper, we present two-dimensional tomographic images along two orthogonal profiles across Deception Island that are obtained from data collected during a three-dimensional seismic tomography experiment. The seismic data are used to assess the distribution of the melt beneath the island, image a regional fault that constrains the location of the volcano, and estimate the size of the caldera forming eruption.

Seismic Experiment and Inversion Method

The seismic data were collected using the *R/V Hesperides* in January 2005 as part of an international experiment led by the University of Granada, Spain. The experiment was designed to obtain a high-resolution three-dimensional image of a volume extending up to ~20 km from the center of the caldera and down to at least ~3 km depth, and also included a 90-km-long NNW-SSE profile for deeper imaging of the crust beneath the island (Figure 1b). For logistical reasons, two rounds of shooting were undertaken with different instrument locations but very similar shot configurations. Data were recorded on three-component geophones at 26 land stations and by 9 compact arrays each of which comprised one 3-component seismometer and between 8 and 20 vertical-component seismometers. Land stations were not deployed uniformly (Figure 1b) due to glacier coverage and the difficult access to parts of the island. Fourteen 1-Hz ocean bottom seismometers (OBS) from the US OBS Instrument Pool were deployed at different locations for each round of shooting at sites within the caldera and around the island. Because of a software problem, data were only obtained from only 14 seafloor sites (Figure 1b).

For shooting we used an array of six airguns with a total volume of 57 liters. In the caldera, shots were fired at a spacing of 120 m on a 0.5 km grid. Outside the caldera shots were fired at a spacing of 170-340 m on three circumferential lines at distances of 10, 15, and 20 km from the center of island and on eight radial lines each of which extended at least 25 km from the center of the island. Two of the radial lines were extended to create the 90-km-long refraction profile. In this paper, we present the results of two-dimensional inversions along the 90 km refraction profile which is oriented NNW-SSE and along a 55-km-long profile oriented WSW-ENE (Figure 1b). Each inversion includes stations and shots within a 4- to 5-km-wide corridor. Three-dimensional inversions for shallow volcano structure are the subject of a separate study (Zandomeneghi et al., 2005).

With the exception of a few intervals when background noise levels increase substantially for unknown reasons, the signal to noise ratio at shorter ranges is high and first arrivals can be picked directly. At ranges exceeding ~30 km, the signal to noise ratio is often low and the first arrivals emergent. This is particularly so for paths that pass beneath the island. To pick arrivals with low signal to noise ratios, we implemented a cross-correlation technique to align groups of adjacent arrivals and made the pick from a stack of aligned arrivals. For all travel time data, we assigned nominal pick uncertainties of 0.01, 0.02, 0.04 or 0.08 s, depending on a qualitative assessment of the pick quality. For the NNW-SSE profile the data set comprises 2793 arrival time picks from 627 shots and 16 stations. For the WSW-ENS profile, there are 1325 arrivals for 280 shots and 11 stations.

We used the marine tomography algorithm of Toomey et al. (1994) which incorporates accurate corrections for the water path that are based on bathymetry, and implements separate grids for the forward ray tracing problem and for the inversion. Both grids are hung from the bathymetry and topography and all of our results are referenced to this surface. For this study, we traced rays through a three-dimensional grid with a spacing of 200m. For the inverse problem a two-dimensional perturbation grid was used with spacing of 500m. We initially used a one-dimensional starting velocity

model based on Christeson et al. (2003), but in subsequent inversions, including those presented in this paper, we used a one-dimensional starting model that is a horizontal average of the tomography result away from the island.

Results

We performed tomographic inversions along each profile with a variety of smoothing and damping weights. The images presented here are our preferred models, although we note that the primary features in the images are insensitive to the choice of inversion parameters and starting models, and to the exclusion of shots lying near the edges of the profile corridors. Along the NNW-SSE profile, the ray coverage extends down to ~9 km with a high density of crossing rays beneath the volcano down to over 4 km depth (Figure 2b). The root mean squared (RMS) travel time residual for the inversion is 57 ms. Five primary features are visible in the image (Figure 2c). There is a low velocity anomaly beneath much of the caldera with a maximum magnitude of -0.7 km/s at a depth of 3.5 km, that is truncated to either side by high-velocity anomalies. To the north, the high velocity anomaly extends over 20 km to the end of the profile. To the south, the high velocity is narrow and partially underlies the southern margin of the caldera. South of Deception Island there is a 30- to 40-km-wide region with generally small negative velocity anomalies. This transitions abruptly to high velocities near the southern end of the profile.

Along the ENE-WSW profile, the ray coverage extends down to ~6 km depth but there are very few crossing rays at depths exceeding 3-4 km. The RMS residual of this inversion is 40 ms. The low velocity anomaly beneath the caldera has a maximum amplitude of -1 km/s at 2.6 km depth and is bounded on either side by narrow high-velocity anomalies that are not as pronounced as in the NNW-ENE profile. The volcano flanks are underlain by negative anomalies.

We used checkerboard tests to assess the resolution of our models. For each profile, we forward modeled the travel times for the same source-receiver configuration as the data, through models comprising alternating blocks of low and high velocity anomalies. These travel time data were then inverted using the tomography algorithm to see what features were retained. The results show that beneath the volcano 2-km-wide features are generally well resolved in the upper 2 km with even higher horizontal resolution in the upper 1 km of the caldera. Features that are 5 km wide are well resolved down to 4 km depth but at larger depths the paucity of crossing rays substantially limits resolution.

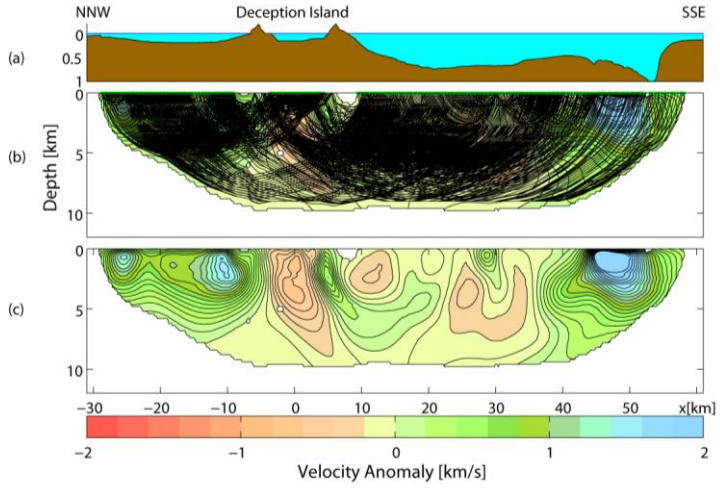

Figure 2. Results of tomographic inversions along the NNW-SSE profile showing (a) the bathymetry along the profile (b) the velocity perturbations overlain by the ray paths and (c) the velocity perturbations. The vertical exaggeration in (b) and (c) is 1.8 and the contour interval is 0.1 km/s.

Discussion

The high gradient between the low velocity anomaly beneath the caldera and the high velocity anomaly to the north of the island coincides with a regional normal fault (Rey et al., 2002) that marks the northern border of extension in Bransfield Strait and coincides with the steep bathymetry gradients visible to the ENE of Deception Island Figure 1a. When extrapolated across Deception Island this fault coincides with the northwestern margin of the caldera and with the line of 1967 and 1970 eruption centers near Telefon Bay (Ibanez et al., 2003). The fault plane may provide a deep conduit for magma to migrate to the volcano and may play a role in constraining its location, although other volcanic centers in the Central Bransfield Basin are not located along the north bounding fault (Gràcia et al., 1997). On the basis of the analysis of magnetic and gravimetric data, Muñoz-Martín et al, (2005) argue that this fault marks the boundary between continental crust to the north of Deception Island and more basic crust to the south. However, at the depth of imaging for our model (< ~5 km), the north to south decrease in velocity across this boundary imaged by our study and previous investigations (Christeson et al., 2003; Grad et al., 1992), presumably reflects a transition from undeformed continental crust to the north to extended crust to the south that is overlain by sediments and volcanics.

The narrow high velocity anomaly observed beneath the southern margin of the caldera in the NNE-SSW profile is not clearly related to any surface feature. It is well imaged at shallower depths but its elongation along the predominant ray path direction suggesting that its base is not well resolved. One possible interpretation is that it is a cooled magmatic intrusion that penetrates to shallow depths.

The wide region of low velocity anomalies south of the island is presumably a region where sediments and volcanic sequences have accumulated in the extensional basin. The high velocity anomaly at the southern end of the NNW-SSE profile is somewhat puzzling since it lies to the north of the southern margin of the basin (this is clearly apparent in the bathymetry of the profile shown in Figure 2a). Barker and Austin (1998) found evidences for magmatic intrusions near the southern margin of the basin and such an explanation would be consistent with high seismic velocities.

In order to understand the origin of the low velocity anomaly beneath the caldera, we first sought to assess the contribution from shallow sediments and unconsolidated volcanics. We analyzed refraction record sections within the caldera after correcting the travel times and shot locations to the ray entry point on the seafloor. The refracted arrivals are fit well by a flat layer model in which a 1.2-km-thick sediment layer with an average velocity of 2.1 km/s overlies a basement layer with a velocity of ~4 km/s. These results are very consistent with the earlier study of Grad et al. (1992). We conducted synthetic inversions in which the sediment layer in the caldera region was superimposed on a one-dimensional starting model. The results show that only a small proportion of the observed low-velocity anomaly is the result of this layer.

We next explored the hypothesis that the sediment layer is underlain by a shallow magma chamber by systematically exploring synthetic models which include both the caldera sediments and an underlying magma chamber of varying dimensions and anomaly size. Figure 3 shows one example of a synthetic test for the NNW-SSE profile that reproduces the basic characteristics of the observed anomaly reasonably well. The synthetic model includes a 4.8-km-wide magma chamber that extends downwards from a depth of 1.4 km, has a constant velocity anomaly of -1.2 km/s in its upper 1 km, and an anomaly that decreases downwards linearly to zero over 8 km. Based on such tests we infer that the top of the magma chamber is at <2 km depth, and that its width is between 3-5 km along the NNW-SSE profile and 2-3 km along the ENE-WSW profile. The base of magma chamber is not well resolved but the synthetic inversions show that a significant velocity anomaly must extend to at least 4-5 km depth.

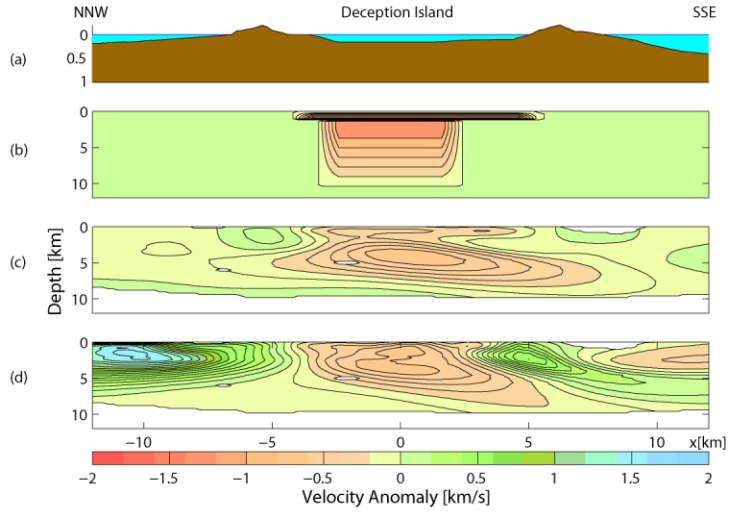

Figure 3. Result of a synthetic test along the NNW-SSE profile for a model with caldera sediments underlain by a magma chamber showing (a) the bathymetry profile, (b) the velocity anomaly for the synthetic stating model, (c) the results of the synthetic inversion, and (d) for comparison, the results of inverting the real data from Figure 2. The contour interval is 0.1 km/s.

The melt fraction in the magma chamber was estimated using a method described by Dunn et al. (2000). For the NNW-SSE profile, the inversion of Figure 2 yields a maximum melt fraction of 4-14%. However, it is clear from the synthetic tests, that the tomographic images underpredict the magnitude of the low velocity anomaly. The starting model for the synthetic test of Figure 3, has an absolute velocity of 2.6 km/s at the top of the magma that is consistent with a fully molten magma chamber and the method of Dunn et al. (2000) suggests that partial melt is present down to about 4.5 km depth.

We have used our constraints on the thickness of the caldera sediment layer to estimate the maximum volume of a caldera forming eruption(s). We approximate the caldera by an ellipse with radii of 4.5 km and 2.7 km and a thickness of 1.4 km (the thickness of the water and sediment layers) and assume that the emerged volcano had a conical shape prior to the eruption and a maximum elevation above sea level of 750 m. This yields a volume of ~60 km^3 which is significantly larger than the previous estimate of 30 km^3 (Smellie et al., 2002).

Acknowledgements. We thank the officers and crew of the *R/V Hespérides* and *R/V Las Palmas*, the scientific party, and personnel of the Gabriel de Castilla base for their assistance collecting the data. We also thank Gail Christeson and co-editor Paul Fitzgerald for reviewing and handling this contribution. This work was supported by the National Science Foundation under grant ANT-0230094 and by the Spanish Tomodec Project (REN 200-3833).

References

Baker, P. E., I. McReath, M. R. Harvey, M. J. Roobol, and T. G. Davies (1975), The geology of the South Shetland Islands; V, Volcanic evolution of Deception Island, Brit. Antarct. Surv. Sci. Rep., 78.

Barker, D. H. N., and J. A. Austin (1998), Rift propagation, detachment faulting, and associated magmatism in Bransfield Strait, Antarctic Peninsula, J. Geophys. Res., 103, 24017-24044.

Barker, P. F. (1982), The Cenozoic subduction history of the Pacific margin of the Antarctic Peninsula: ridge crest-trench interactions, J. Geol. Soc. London, 139, 787–801.

Christeson, G. L., D. H. N. Barker, J. A. Austin, and I. W. D. Dalziel (2003), Deep crustal structure of Bransfield Strait: Initiation of a back arc basin by rift reactivation and propagation, J. Geophys. Res., DOI: 10.1029/2003JB002468.

Dunn, R. A., D. R. Toomey, and S. C. Solomon (2000), Three-dimensional seismic structure and physical properties of the crust and shallow mantle beneath the East Pacific Rise at 9 30'N, J. Geophys. Res., 105, 23537-23556.

Gràcia, E., M. Canals, M. L. Farràn, J. Sorribas, and R. Pallàs (1997), Central and eastern Bransfield basins (Antarctica) from high-resolution swath-bathymetry data, Antarct. Sci., 9, 168-180.

Grad, M., A. Guterch, and P. Sroda (1992), Upper crustal structure of Deception Island area, Bransfield Strait, West Antarctica, Antarct. Sci., 4, 469-476.

Grad, M., H. Shiobara, T. Janik, A. Guterch, and H. Shimamura (1997), Crustal model of the Bransfield Rift, West Antarctica, from detailed OBS refraction experiments, Geophys. J. Int., 130, 506-518.

Ibanez, J. M., J. Almendros, E. Carmona, C. Martnez-Arevalo, and M. Abril (2003), The recent seismo-volcanic activity at Deception Island volcano, Deep Sea Research Part II: Topical Studies in Oceanography, 50, 1611-1629.

Marti, J., J. Vila, and J. Rey (1996), Deception Island (Bransfield Strait, Antarctica); an example of a volcanic caldera developed by extensional tectonics, Geological Society Special Publications, 110, 253-265.

Muñoz-Martín, A., M. Catalán, J. Martín-Dávila, and A. Carbo (2005), Upper crustal structure of Deception Island area (Bransfield Strait, Antarctica) from gravity and magnetic modeling, Antarct. Sci., 17, 213-224.

Ortiz, R., J. Vila, A. Garcia, A. G. Camacho, J. L. Diez, A. Aparicio, R. Soto, J. G. Viramonte, C. Risso, and N. Menegatti (1991), Geophysical features of Deception Island, International Symposium on Antarctic Earth Sciences, 6, 461-463.

Rey, J., A. Maestro, L. Somoza, and S. J.L. (2002), Submarine morphology and seismic stratigraphy of Port Foster, in Geology and geomorphology of Deception Island, edited by J. Lopez-Martinez, et al., pp. 40-46, British Antarctic Survey.

Robertson, S. D., D. A. Wiens, P. J. Shore, G. P. Smith, and E. Vera (2002), Seismicity and tectonics of the South Shetland Islands and Bransfield Strait from the SEPA broadband seismograph deployment, Bulletin - Royal Society of New Zealand, 35, 549-554.

Smellie, J. L. (2001), Lithostratigraphy and volcanic evolution of Deception Island, South Shetland Islands, Antarct. Sci., 13, 188-209.

Smellie, J. L., J. L. Martínez, and B. A. Survey (2002), Geology and Geomorphology of Deception Island, British Antarctic Survey.

Toomey, D. R., S. C. Solomon, and G. M. Purdy (1994), Tomographic imaging of the shallow crustal structure of the East Pacific Rise at 9 deg 30 min N, J. Geophys. Res., 99, 24,135-124,157.

Zandomeneghi, D., J. Almendros, A. Barclay, and J. M. Ibáñez (2005), Preliminary Seismic Tomography of Deception Island Volcano, South Shetland Islands (Antarctica), Eos Trans. AGU, Fall meet. Suppl., Abstract S41A-0975.